Equilibrium and Transient Climate Response to Anthropogenic Forcing: the Impact of Atmospheric Feedback Processes

Minghua Zhang

School of Marine and Atmopsheric Sciences

State University of New York at Stony Brook, NY 11794

Email: Minghua.Zhang@stonybrook.edu

Transactions of Atmospheric Sciences
Vol. 34 No. 3, Jun. 2011

In dedication to Professor Qian-gen Zhu

2010

ABSTRACT

Coupled ocean-land-atmospheric general circulation models are the only tools to quantitatively attribute past climate change in response to human activities and to predict the magnitude of future climate change. These models are known to differ considerably in their equilibrium sensitivities to external forcing, largely because of differences in atmospheric feedbacks, especially in cloud-climate feedbacks. Yet, all models that participated in the IPCC (Inter-governmental Panel on Climate Change) Assessment Report (AR4) showed very similar simulations of the 20th century climate by these models. This paper investigates the causes and implications of this similarity. It shows three equally important physical mechanisms acting together to reduce the sensitivity of transient climate change to model differences. These include the longer time delay of climate response to forcing, more heat exchange with the deep ocean, and larger impact of oceanic upwelling in models with larger atmospheric feedbacks. However, inter-model differences will show up at longer time scales. This study also shows that under mitigation scenarios of greenhouse gases, climate warming can continue for longer time after their radiative forcing reaches maximum in the more sensitive climate models.

1. Introduction

Climate sensitivity refers to the change of globally averaged surface temperature in response to a specified external forcing. Because of the increasing amount of atmospheric greenhouse gases as a result of human use of fossil fuels, understanding the magnitude of the response of surface temperature to anthropogenic activities, and thus the sensitivity of the climate system, has been an active area of research in the last thirty years (Randall et al. 2007).

Coupled General Circulation Models (CGCMs) are one of the few available tools to derive the climate sensitivity. Earlier studies used atmospheric models with mixed layer oceans to derive it by integrating a model to equilibrium state under constant forcing (e.g., Hansen et al. 1984; Wetherald and Manabe 1988). This sensitivity is referred to as the equilibrium sensitivity of a climate model. It has been known that atmospheric feedback processes, especially cloud- feedback, play a major role in determining the sensitivity of the climate system or a climate model (Cess et al. 1990; Senior and Mitchell 1993). The discrepancies in cloud feedbacks among the models imply several factors of difference in climate responses from these models to the radiative forcing from a doubling of CO_2 concentration in the atmosphere, which is about 3.7 W/m^2 (Andreae 2005).

Results from the multi-model ensemble of IPCC AR4 however showed that different climate models simulated similar magnitudes of global temperature change for the 20^{th}

century (Meehl et al. 2007), even though their atmospheric feedback processes are very different (Soden and Held 2006; Defresne and Bony 2008). As an example, Figure 1a shows the changes of temperature in the 140 years from 1860 to 2000 simulated by using two CGCMs, one from the National Center for Atmospheric Research (NCAR) version CCSM3, and the other from the Geophysical Fluid Dynamics Laboratory (GFDL) version CM2. Also plotted is the observed temperature variation during this period (Brohan et al. 2006). The best estimates of climate forcing, from greenhouse gases alone, from the combination of greenhouse gases and tropospheric aerosol, and from all sources (including greenhouse gases, tropospheric aerosol, solar activities, and volcanic aerosols) are shown in Figure 1b (Hansen 2001). The human industrialization has created a greenhouse forcing of about 2.5 W/m^2; this is offset by about 1 W/m^2 from increased aerosol loading in the troposphere during the same period, leading to a total net forcing of about 1.5 W/m^2 with other components to be relatively small. The two models in Figure 1a used a variant of the forcing in Figure 1b.

These two models are known to have different cloud-climate feedbacks: the NCAR CCSM3 has a negative cloud feedback; while the GFDL AM2 has a positive cloud feedback (Wyant et al. 2006). This is shown in Figure 2, in terms of the change of cloud radiative forcing at the top of the atmosphere (TOA) normalized to a unit change of surface temperature. Averaged from 60^oS to 60^oN, the changes of clouds in the NCAR CCSM have the effect of losing 1.2 W/m^2 of energy for one degree change of surface temperature, while cloud changes in the model GFDL CM model have the effect of a 0.2 W/m^2 gain of radiative energy. Combining these values with the approximate 0.7^oK

climate change, one can infer the forcing from the sum of the externally imposed forcing and the cloud forcing in the CCSM to be about 0.5 W/m^2, much less than the 1.5 W/m^2 in Figure 1b, while that in the GFDL CM to larger than 1.6 W/m^2. Given these differences, how can the two models both simulate similar climate for the 20th century?

This paper investigates the impact of atmospheric feedbacks on the transient climate response to external forcing. The purpose is to answer the simple question: will models with different equilibrium climate sensitivities produce similar 20th century climate from the observed forcing? Answer to this question will provide guidance about what factors are the most important in determining climate change in the time horizon of several decades to a century. It will additionally address whether cloud feedback can be inferred from modern instrument records.

Kiehl (2007) used results from an ensemble of models to investigate the same question. He postulated that the different models must have used different aerosol loading in their forcing, such that models of high sensitivity (positive cloud feedback) might have contained larger aerosol cooling effects while models of low sensitivity (negative cloud feedback) might have contained smaller aerosol cooling effects. We will show that there are other underlying physical reasons to explain the simulated climate change for the 20th century from different models.

In the following, I will first describe a model in Section 2 and then the terminology of forcing and sensitivity in Section 3. Results are presented in Section 4, first for a special case and then for a more general case. The last section contains a summary of the paper.

2. The Model

The atmosphere is described by a simple energy balance model averaged over the whole atmosphere written for a unit surface area as

$$\frac{\partial h_a}{\partial t} = N_s - N_T \tag{1}$$

where h_a is the moist static energy of the atmosphere:

$$h_a = \int_{p_t}^{p_s} (C_p T_a + gz + L\,q)\frac{dp}{g}. \tag{2}$$

N_S and N_T denote the net upward energy flux at the surface and top-of-the-model (TOM) respectively with surface pressure p_s and TOM pressure p_t; T_a, z, q are air temperature, height, and water vapor mixing ration; C_p, g, and L are specific heat of air under constant pressure, gravitational constant, and latent heat of evaporation or condensation. Equation (1) is valid for a hydrostatic atmosphere. p_t does not have to be the real top of the atmosphere. Instead, it is often selected at a level where external forcing is defined.

The Earth surface is assumed to be covered by water with a mixed layer of depth D. The mixed-layer thermodynamic equation is

$$c_w \rho_w D\left(\frac{\partial T_s}{\partial t} + u_s \frac{\partial T_s}{\partial x} + v_s \frac{\partial T_s}{\partial y}\right) = -N_s + N_D \tag{3}$$

where T_s is the mixed-layer temperature, which we refer to as the sea surface temperature (SST), u_s and v_s are horizontal currents, c_w and ρ_w are the specific heat and density of sea water. N_D is the upward heat flux at the bottom of the mixed layer. This heat flux can be expressed in terms of entrainment velocity w_e at the bottom of the ocean mixed layer, just like the turbulent entrainment of heat and moisture at the top of atmospheric boundary layer (e.g., Lilly 1968). It is written as

$$N_D = c_w \rho_w \overline{w'T'}|_{z=-D} = -c_w \rho_w w_e (T_s - T_0) \tag{4}$$

where T_0 is the deep water temperature immediately below the mixed layer.

Below the mixed layer for $z < -D$, the ocean temperature is controlled by

$$\frac{\partial T}{\partial t} + u\frac{\partial T}{\partial x} + v\frac{\partial T}{\partial y} + w\frac{\partial T}{\partial z} = \frac{\partial}{\partial z}(k\frac{\partial T}{\partial z}) \tag{5}$$

where k is the vertical diffusivity; u, v and w are velocity components of the ocean currents. The upper boundary condition of the deep ocean is

$$c_w \rho_w k \frac{\partial T}{\partial z} = -\mathrm{N_D} \text{ for } z = -D. \tag{6}$$

The other boundary condition is at the bottom of the deep ocean and it can assume two forms: one with no heat flux, and the other with fixed temperature, corresponding to a Dirichlet or Neumann boundary conditions:

$$\frac{\partial T}{\partial z} = 0 \text{ for } z = -H \tag{7}$$

or

$$T = T_b \text{ for } z = -H \tag{8}$$

where H is the depth of the ocean. A more accurate boundary condition at the bottom of the ocean is to make the net heat flux equal to the thermal flux of the Earth crust, but this

would introduce additional variables. For practical purposes of studying climate change on the time scale of less than a few centuries, (7) and (8) are equally valid since heat diffusion into the deep ocean is a very slow process. These assumptions are equivalent to setting the ocean to an infinite depth for the study of a forced solution from the atmosphere. Therefore, in the following study, we will use $H=-\infty$.

The governing equations of (1), (3) and (5) describe the three components – atmosphere, SST, and a deep ocean – of the climate system under external forcing through the atmosphere. These components are schematically shown in Figure 3. Similar models have been used in previous studies (e.g., Cess and Goldenberg 1981; Raper et al. 2001; Wigley 2005), but for different purposes. This paper will be only concerned with the tropical region, since it occupies the largest portion of the surface. For simplicity, horizontal transport of heat in this region is neglected, and upwelling is specified.

The coupling between the atmosphere and the mixed layer ocean is through the net surface heat flux N_s; the coupling between the mixed layer and the deep ocean is through the turbulent heat flux at the bottom of the mixed layer N_D. Combining (1) and (3) without the ocean currents would yield the heat budget equation for the atmosphere and the ocean mixed-layer:

$$\frac{\partial}{\partial t}\left[\int_{p_t}^{p_s}(C_p T_a + gz + L\,q)\frac{dp}{g} + c_w \rho_w D T_s\right] = -N_T + N_D. \qquad (9)$$

3. Climate forcing and sensitivity

a. formulation of forcing and feedback

The TOM net upward heat flux N_T in (9) is the sum of shortwave and infrared longwave radiation. It is only a function of the surface temperature and atmospheric state. We can functionally write it as

$$N_T = N\left(T_s, T_a - T_s, q, q_{CO_2}, sea\ ice, aerosol, clouds, solar\right) \qquad (10)$$

where T_a and q are the three-dimensional air temperature and water vapor respectively; q_{CO_2} represents greenhouse gas concentration; other variables are self explanatory.

To study climate change under an external forcing, all state variables are written as perturbation to a reference state. The above equation can be linearized as

$$N_T = \frac{\partial N}{\partial T_s}T_s + \frac{\partial N}{\partial (T_a - T_s)}(T_a - T_s) + \frac{\partial N}{\partial q}q + \frac{\partial N}{\partial q_{CO2}}q_{CO_2} + \frac{\partial N}{\partial (sea\ ice)}(sea\ ice) + \frac{\partial N}{\partial (aerosols)}(aerosol) + \frac{\partial N}{\partial (clouds)}(clouds) + \frac{\partial N}{\partial (solar)}solar. \qquad (11)$$

All partial derivatives are taken at the reference state, such as the current climatological condition. We have used CO_2 as a surrogate for all greenhouse gases.

Climate forcing can be imposed by changes in the anthropogenic or natural event-driven independent variables. The anthropogenic forcing includes atmospheric greenhouse gas and aerosol forcing, while the natural forcing includes solar variability. These forcing terms are combined together as a total forcing written as a downward radiative flux:

$$F = -\frac{\partial N_T}{\partial q_{CO2}}q_{CO_2} - \frac{\partial N_T}{\partial (aerosol)}(aerosol) - \frac{\partial N_T}{\partial (solar)}(solar). \qquad (12)$$

All other terms in equation (11) represent atmospheric feedback processes, often expressed using the surface temperature as the control variable. They include the negative Stefan-Boltzman radiative feedback, temperature lapse-rate feedback, water vapor feedback, snow and sea-ice feedback, and cloud feedback (e.g., Schelinger 1988), which can combined as

$$Q = \frac{\partial N_T}{\partial T_s}\Delta T_s + \frac{\partial N_T}{\partial (T_a - T_s)}\frac{\partial (T_a - T_s)}{\partial T_s}\Delta T_s + \frac{\partial N_T}{\partial q}\frac{\partial q}{\partial T_s}\Delta T_s + \frac{\partial N_T}{\partial (clouds)}\frac{\partial (clouds)}{\partial T_s}\Delta T_s + \cdots. \quad (13)$$

The symbol Δ is added for clarity in this expression only. The coefficients of the partial derivatives to each independent variable are called as the radiative kernels in Soden et al. (2008); these are found to be somewhat independent of which climate model is used. The coefficients of ΔT_s are called feedbacks, in units of (W/m^2)/K.

To isolate the cloud feedback, we will combine the Stefan-Boltzman term and those from temperature lapse rate, water vapor, snow/sea ice into a single parameter, λ_0, expressed as W/m^2/K, and write the cloud feedback as the change of cloud-radiative forcing (downward) as λ_c. Thus,

$$Q = (\lambda_0 - \lambda_c)T_s \quad (14)$$

where

$$\lambda_c = -\frac{\partial N_T}{\partial (clouds)}\frac{\partial (clouds)}{\partial T_s} = \frac{\Delta CRF^*}{\Delta T_s}. \quad (15)$$

This cloud feedback represents the increase of net downward radiation at TOA due to change of clouds associated with a unit change of surface temperature.

A more widely used definition of cloud-radiative forcing, denoted by CRF, is the difference of total-sky N_T and clear-sky radiative flux N_{TC} (Ramanathan 1987):

$$CRF \quad = N_{TC} - N_T \tag{16}$$

$$\Delta CRF \quad = \Delta N_{TC} - \Delta N_T \tag{17}$$

This definition differs slightly from that in (15). The two are related with each other through

$$\Delta CRF^* = \Delta CRF - \left(\frac{dN_T}{dT_s}|_{clouds=0} - \frac{dN_T}{dT_s}|_{clouds}\right)\Delta T_s. \tag{18}$$

We will not devolve further into this distinction; interested readers are referred to Soden et al. (2004) for additional discussions.

The net upward TOM radiative flux N_T in (11) can thus be written as

$$N_T = -F + (\lambda_0 - \lambda_c)T_s \tag{19}$$

where the first term on the right hand side is the climate forcing; the second term is the atmospheric feedbacks. A positive $\lambda_c$represents positive cloud feedback, while a negative $\lambda_c$represents a negative cloud feedback. It should be noted that in terms of difference among climate models, we can consider $\lambda_0$to be the ensemble mean of all terms in (13) and λ_c to represent all intermodal differences. But for ease of description, we refer to the latter it as cloud feedback.

b. terminology and specification

In the energy budget equation (9) for the atmosphere and the ocean mixed layer, if we assume an ocean mixed layer of 75 meters (e.g., Liu et al. 2010), on the left hand side of equation (9), the coefficient for the oceanic term is $c_w\rho_w D$=3×10^8 J/K, while the coefficient of the atmospheric term is on the order of $C_p \times p_s/g$ = 1×10^7 J/K. Therefore,

the atmospheric term can be neglected. This is equivalent to assume a zero heat capacity atmosphere, but the atmosphere is needed to introduce the climate forcing. Together with equation (4), the controlling equation of SST can be written as

$$c_w \rho_w D \frac{\partial T_s}{\partial t} = F - (\lambda_0 - \lambda_c) T_s - c_w \rho_w w_e (T_s - T_0). \quad (20)$$

The terms on the right hand of (20) describe the climate forcing, atmospheric feedbacks, and mixing of heat with the deep ocean.

We next introduce the terminology of climate sensitivity and response. The equilibrium sensitivity is in theory only defined when the forcing in (20) is steady, i.e., independent of time. It refers to the magnitude of SST change under a unit external forcing. By setting the time derivatives in (5) and (20) to zero, one can get the steady state solution of the model and obtain the *equilibrium climate sensitivity* δ_e with respect to unit forcing as:

$$\delta_e = \frac{T_s}{F} = \frac{1}{(\lambda_0 - \lambda_c)}. \quad (21)$$

δ_e is an inherent property of the climate system rather than the forcing, thus the definition of equilibrium can be used even if the forcing varies with time.

Under time-varying external forcing *F(t)*, the *equilibrium temperature response*, denoted as T_{se}, is defined as the product of the equilibrium sensitivity (21) and the transient forcing:

$$T_{se}(t) = F(t)\delta_e. \quad (22)$$

This is equivalent to a hypothetical solution by setting all time derivative terms in (20) and (5) to zero.

The true solution of (5) and (20) is used to define the so-called *transient climate sensitivity* with respect to a unit forcing.

$$\delta_t = \frac{\mathrm{T_s(t)}}{F(t)}. \tag{23}$$

The *transient climate response* is, by definition,

$$T_s(t) = F(t)\delta_t. \tag{24}$$

We will use a heuristic forcing scenario in this study. Anthropogenic climate forcing is assumed to increase at a rate of 0.04 W/m^2 per year, leading to 4 W/m^2 per century, for the first fifty years. This rate of change in forcing is comparable to the IPCC A1B scenario shown in Figure 4a (Forster et al. 2007). After fifty years, the forcing is assumed to decrease to zero within a century (Figure 4b). The IPCC best emission scenario B1 is shown in Figure 4a as a reference. The adopted mitigation scenario in Figure 4b is much more aggressive than what can be expected in reality and it is used only to understand the behavior of solution under a strong policy action on greenhouse gases.

4. Results

The exchange of heat between the mixed layer and the deep ocean is equivalent to an increase of the heat capacity of the mixed layer, but this increase is related with how temperature changes in the deep ocean as described in (20).

We will shift the vertical coordinate to make the bottom of the mixed layer as *z=0* . Given the upper boundary condition of the deep ocean as a function of time $T|_{z=0} = T_0(t)$, the solution of the deep ocean temperature equation (5), without the horizontal currents, can be obtained using Laplace transform in time *t* as:

$$T(t,z) = \int_0^t T_0(t') \frac{\mathrm{d}}{\mathrm{d}t'} [\mathrm{erfc}\left(\frac{z-wt}{\sqrt{4k(t-t')}}\right)]\, dt', \tag{25}$$

where *erfc* is the complimentary error function defined as

$$erfc(x) = 1 - \frac{2}{\sqrt{\pi}} \int_0^x \exp(-\xi^2)\, d\xi.$$

For the solution of $T_0(t)$, the boundary conditions of (4) and (6), relating the diffusive heat flux with the entrainment flux at the top of the deep ocean, can be used so that

$$\int_0^t T_0(t')\, G(t',t)\, dt' = \frac{w_e}{k} (T_s - T_0)\ , \tag{26}$$

where

$$G(t',t) = \frac{\partial}{\partial z} \left[\frac{\mathrm{d}}{\mathrm{d}t'} \mathrm{erfc}\left(\frac{z-w(t-t')}{\sqrt{4k(t-t')}}\right)\right] |_{z=0}. \tag{27}$$

Thus,

$$T_0 = (£ + 1)^{-1} T_s \tag{28}$$

where £ is an integral operator, which is a triangular matrix in practical calculations:

$$£\psi = \frac{k}{w_e} \int_0^t G(t',t)\psi(t')\, dt' \tag{29}$$

Using (28), the equation for SST in (20) can be written as

$$c_w \rho_w D \frac{\partial T_s}{\partial t} = F - (\lambda_0 - \lambda_c) T_s - c_w \rho_w w_e [1 - (£ + 1)^{-1}] T_s. \tag{30}$$

Unlike the atmospheric feedback that is directly proportional to the SST at a given time, the heat flux into the ocean depends on the time history of the SST that is in turn a

function of the forcing. Furthermore, this heat flux, depending on the evolution of the SST history, may change sign even if the SST perturbation at the given time is positive. Equation (30) can be integrated forward with time by using the forcing and past history of T_s.

a. a special case without deep ocean

We first examine the SST response to a specified climate forcing without a deep ocean. This is equivalent to setting the entrainment velocity to zero, and thus the last term in Equation (30) to zero. From the terminology defined in the previous section, the equilibrium climate response, written as T_{se}, is:

$$T_{se}(t) = \frac{F(t)}{(\lambda_0 - \lambda_c)}. \tag{31}$$

The sensitivity of the equilibrium response to cloud feedback can be written as

$$\delta T_{se} = \frac{F}{(\lambda_0 - \lambda_c)^2}\delta\lambda_c. \tag{32}$$

or

$$\frac{\delta T_{se}}{T_{se}} = -\frac{\delta(\lambda_0 - \lambda_c)}{(\lambda_0 - \lambda_c)} = \frac{\delta\lambda_c}{(\lambda_0 - \lambda_c)}. \tag{33}$$

The percent change of the equilibrium response with respect to a unit change in cloud feedback is equal to the equilibrium sensitivity itself. Therefore, with a positive cloud feedback ($\lambda_c > 0$), a small change in the cloud feedback can cause large change in the magnitude of the response. On the other hand, if the cloud feedback is negative ($\lambda_c < 0$), T_{se} is small, an uncertainty in cloud feedback causes much smaller temperature change.

For the atmospheric feedbacks, we will take λ_0 as 1.35 W/m^2/K, corresponding to 2 K climate change from a doubling of CO_2 without cloud feedback (Hansen et al. 1984; Schlesinger 1988). This value is mainly contributed by the negative Stefan-Boltzman feedback and the positive water vapor feedback, which can be estimated based on constant relative humidity of the atmosphere. The dashed lines in Figure 5 show the equilibrium response of the SST to the specified forcing in Figure 4b, plotted with cloud feedbacks of $\lambda_{c.}$ as -0.75 (blue), 0 (black), and 0.75 (red) W/m^2/K respectively to resemble the range in the current generation of CGCMs (Cess et al. 1990; Soden and Held 2006). The top panel is for the first fifty years; the bottom panel is for the entire 150 years. As expected, time variations of the equilibrium response simply follow that of the forcing. This will be contrasted with those of the transient SST response below. The spacing between the responses with $\lambda_c = 0$ and $\lambda_c = 0.75$ is much larger than that between $\lambda_c = 0$ and $\lambda_c = -0.75$.

For the transient SST response in the fifty years when the forcing is $F(t) = \alpha t$, the solution of (30) is

$$T_s(t) = \frac{\alpha\,(t-\tau)}{(\lambda_0-\lambda_c)} + \frac{\alpha\,\tau_1^2}{C}\,e^{-\frac{t}{\tau}}. \tag{34}$$

where

$$\tau = \frac{C}{(\lambda_0-\lambda_c)}, \quad C = c_w\rho_w D. \tag{35}$$

τ is the time scale of the response. The second term in (34) can be neglected when t>>τ. The first term is the equilibrium temperature response with a time delay τ_1. This delay in the response has been reported in previous research (e.g., Cess and Goldenberg 1981;

Bao and Zhang 1991). But what can be seen is that the larger the cloud feedback, the longer is the delay. For a mixed-layer depth of 75 m, with cloud feedback of -0.75, 0, and 0.75 W/m^2/K, the time scale τ_1 is 5 years, 7 years and 16 years respectively.

The solid lines in Figure 5 show the transient response of SST corresponding to the three cloud feedbacks. Notice that after t>>20 years, the temperature response for all cloud feedbacks is almost parallel to the corresponding equilibrium SST responses (the dashed lines), but with a delay that is proportional to cloud feedback. Because of the difference in delay, however, the sensitivity of temperature response to cloud feedback at the initial time t < 20 is small, which can be clearly seen in Figure 5a. This can be also shown analytically from (34), after some manipulation, as:

$$\frac{\partial \mathrm{T_s}}{\partial \lambda_c} = \beta(t,\tau)\frac{\partial \mathrm{T_{se}}}{\partial \lambda_c}, \tag{36}$$

where

$$\beta(t,\tau)=(1-\frac{2\tau}{t})(1+\frac{2\tau}{t})e^{-\frac{t}{\tau}} = \frac{1}{6}(\frac{\tau}{t})^2 - \frac{1}{12}(\frac{\tau}{t})^3 + \frac{1}{40}(\frac{\tau}{t})^4 + \cdots \tag{37}$$

When t=τ, the transient sensitivity is only about 0.1, one tenth of that of equilibrium sensitivity. For t=2 $\tau, 5\tau, 10\tau$, this factor is 0.27, 0.61, and 0.81 respectively.

After the first fifty years, aside from the time delay, three points are noteworthy in Figure 5b: First, the peak of temperature response occurs after the forcing reaches its peak. Second, the transient climate sensitivity can become larger than the equilibrium sensitivity. Third, the impact of cloud feedback on the transient SST response can be larger than that of the equilibrium response. Therefore, although models may appear to

agree with each other at the beginning, their differences will show up even when the forcing is abated.

The continuing larger increase of temperature after the forcing starts to decrease in the case of positive cloud feedback is somewhat counter-intuitive. But this can be understood as follows: when cloud feedback is large, the ability of the system to emit heat is inefficient. As a result, even after the forcing reaches a peak, the forcing is still larger than the heat loss from the atmospheric feedback; temperature thus continues to rise until the atmospheric feedback is larger enough to offset the reduced forcing.

b. the general case with deep ocean

With a deep ocean, the SST will be also affected by the third term in equation (30). In the following, the entrainment velocity w_e is taken as 10^{-5} m/s. This is in the range of observational derived values (Ostrovskii and Piterbarg, 2000). The thermal diffusivity of heat k in the deep ocean is taken as 10^{-4} m^2/s which is similar to what has been used in the past in CGCMS and in simple energy balance models (e.g., Bao and Zhang 1991). The upwelling velocity of the tropical ocean is set at zero or constant at $w= 10$ m/year (Raper et al. 2001). Sensitivity of results to these parameters will be shown later in this paper.

Figure 6a shows a comparison of the transient response (solid line) with the equilibrium response when the deep ocean is considered for the three values of the cloud feedbacks and no upwelling is assumed. It is seen that the deep ocean affects the SST response in

two ways: it reduces the magnitude of the SST change; it desensitizes the role of cloud feedback. In the time horizon of 150 years, the impact is not just a time delay, but in the slope of the temperature response.

These two effects can be understood from equation (30): the exchange of heat with the deep ocean serves as a sink of energy, similar to the loss of energy through the top of the atmosphere (e.g., Schwartz 2007). This can more clearly seen in Figure 6b which shows the four terms in (30). The forcing (green), offset by the total atmospheric negative feedback (dashed lines) and by the energy input to the deep ocean (solid lines), gives the temperature tendency (dotted lines). Note the impact of cloud feedback: a positive cloud feedback leads to less atmospheric energy loss to space (dashed red line), but more into the deep ocean (solid red). These two terms compensate each other, and as a result, the sensitivity of temperature response to cloud feedback is significantly reduced.

It is also noted that the heat loss to the deep ocean cannot be simply parameterized as an equivalent heat capacity itself in equation (30). This is shown in the scatter plot of the heat flux to the deep ocean against the heat storage term in Figure 7 for the positive and negative cloud feedback. The slope not only changes with time, but also with cloud feedback.

The heat budgets in Figure 6b additionally shows that the ocean can be a source of heat to the surface temperature after the forcing starts to decline. This is due to the warm deep water responding to prior large forcing. Figure 8 shows the vertical distribution of

temperature change in the deep ocean for every twenty years. After the forcing starts to decline, the temperature below the mixed layer can be larger than the SST, supplying heat to the mixed layer. This effect is larger for a positive feedback. As a result, the effect of cloud feedback on the SST response is further delayed.

c. sensitivity to entrainment, diffusivity and upwelling

We next explore the above results as functions of the parameters of the model: the entrainment velocity, the heat diffusivity of the deep ocean, and the upwelling velocity. Figure 9a shows results when the entrainment velocity w_e is reduced by a half, from 10×10^{-6} m/s to 5×10^{-6} m/year, for the three cloud feedbacks. The solid lines represent the control case with $w_e=10\times10^{-6}$ m/s. There is very little change in the responses. With a smaller entrainment velocity, the coefficient of the heat flux to the deep ocean is smaller, but the temperature difference between the mixed layer and the top layer of the deep ocean becomes larger. As a consequence, the total heat flux to the deep ocean changes little.

The results for a reduction of the diffusivity by half, from 1.0×10^{-4} m^2/s to 0.5×10^{-4} m^2/s, are shown in Figure 9b with the solid lines as the control case. A smaller diffusivity leads to larger SST response to external forcing (dashed lines), since the heat cannot be effectively propagated downward. This can be seen in Figure 10a which shows the vertical distribution of deep ocean temperature for a positive cloud feedback case. Comparing the deep water temperature in the control case (solid lines) with that when

diffusivity is reduced by a half (dashed lines), one can see the larger vertical gradient of temperature when diffusivity is smaller, and the colder deep ocean. The diffusivity is therefore an important control parameter of the SST response.

We finally show the impact of the upwelling on the system sensitivity. Given an upwelling velocity of 10 m/year, the temperature response is shown in the dashed lines in Figure 9c. Relative to the control case with no upwelling, the magnitude of SST is reduced, so is the sensitivity to cloud feedback. This reduction is due to a larger leak of heat flux into the ocean, since the ocean is cooled by the upwelling.

The vertical profiles of the ocean temperature for the positive cloud feedback are shown in Figure 10b (dashed lines). The temperature signature in deep ocean is reduced, yielding profiles in the interior of the ocean similar to that from the reduction of the diffusivity. At the ocean surface however, the temperature rise in the upwelling case is much smaller than that when the diffusivity is reduced. In the upwelling case, heat is removed, while in the case of reduced diffusivity, heat is piled near the top. In reality, heat loss due to upwelling will be horizontally advected to higher latitudes, thus propagating the cloud feedback in lower latitudes to middle latitude and polar regions.

6. Summary

The above analyses show that the impact of atmospheric feedback (mainly cloud feedback) on the transient climate sensitivity is considerably smaller than that on the

equilibrium sensitivity in the initial stages of an imposed external forcing. This is due to three causes that reinforce each other: (1) The transient climate response has a delay to external forcing, and the delay time increases with cloud feedback; (2) The mixing of heat with the deep ocean removes heat from the forcing, which is larger than for a positive cloud feedback; (3) The upwelling in the tropical ocean promotes further leakage of heat to the deep ocean. These causes do not vary much for different entrainment velocities, but are sensitive to the heat diffusivity of the deep ocean. For plausible values of the entrainment rates and diffusivity in current climate models, all these three causes are equally important.

These results can explain why climate models, even though they have very different cloud feedbacks and equilibrium sensitivities, exhibit little discrepancies in their simulation of the 20^{th} century climate.

Our results do not diminish the importance of cloud feedback in the climate response to external forcing. Instead, it shows how different cloud feedbacks will be propagated through the climate system, and how difference or uncertainties in atmospheric feedbacks will be delayed on long time scales. Furthermore, the transient sensitivity can be larger than equilibrium sensitivity when the forcing starts to decline. Additionally, the temperature response can continue to increase after the peak forcing, especially when the cloud feedback is positive. Finally, the history of the forcing is important to control the magnitude of climate response at any time, which has policy relevance to the negotiation of carbon emissions in the international community.

There are two implications of this study. First, it is unlikely to directly infer cloud feedbacks from observations until after a long time of the forcing, since the initial signal of cloud feedback is weak. Second, in addition to cloud feedback uncertainties, accurate depiction of turbulent mixing within the deep ocean is at least as important as the cloud feedback for transient climate change on the time scale of centuries, even though for equilibrium climate change or on longer time scales, atmospheric feedback is the decidedly more important factor.

Acknowledgements: This paper is dedicated to Prof. Qiangen Zhu, former President of the Nanjing Institute of Meteorology. His past mentorship, support, and kind heart have been a constant source of my gratification. His scientific pursuit in meteorology with rigor and passion, of always combing theory and observations, has been an invaluable inspiration. This research is partially supported by the US Department of Energy under its Climate Change Prediction Program (CCPP) through the FASTER project and by the US National Administration of Space and Aeronautics (NASA) under its Modeling and Analysis Program (MAP). The two climate modeling groups at NCAR and GFDL as well as the Program for Climate Model Diagnosis and Intercomparison (PCMDI) at the Lawrence Livermore National Laboratory (LLNL) are also acknowledged for their climate model simulations.

References

Andreae, M. O., C. D. Jones, and P. M. Cox, 2005: Strong present-day aerosol cooling implies a hot future, Nature, 435, 1187–1190.

Bao N. and X. H. Zhang 1991: Ocean Thermal Diffusivity on Global Induced by Increasing Atmospheric CO2. Adv. In Atmos. Sci., Vol. 8, No. 4.

Brohan P, J. Kennedy, I. Harris I, S. Tett, and P. D. Jones, 2006: Uncertainty estimates in regional and global observed temperature changes: A new data set from 1850, J. Geophys. Res., 111, D12106, doi:10.1029/2005JD006548.

Cess, R.D., and S.D. Goldenberg, 1981: The effect of ocean heat capacity upon global warming due to increasing atmospheric carbon dioxide, *J. Geophys. Res.*, 86: el, 498-502.

Cess, R. D. et al., 1990: J Intercomparison and interpretation of climate feedback processes in 19 atmospheric general circulation models. *J. Geophys. Res*., 95, 16,601-16,615.

Dufresne, J. L., S. Bony, 2008: An Assessment of the Primary Sources of Spread of Global Warming Estimates from Coupled Atmosphere–Ocean Models. *J. Climate*, 21, 5135–5144.

Forster, P., V. et al, 2007: Changes in Atmospheric Constituents and in Radiative Forcing. In: Climate Change 2007: The Physical Science Basis. Contribution of Working Group I to the Fourth Assessment Report of the Intergovernmental Panel on Climate Change [Solomon, S., D. Qin, M. Manning, Z. Chen, M. Marquis,

K.B. Averyt, M.Tignor and H.L. Miller (eds.)]. Cambridge University Press, Cambridge, United Kingdom and New York, NY, USA.

Hansen, J., et al., 1984: Climate sensitivity: analysis of feedback mechanisms, in *Climate Processes and Climate Sensitivity*, Maurice Ewing Series, 5, Edited by J. E. Hansen and T. Takahashi, American Geophysical Union, Washington, D. C., 130-163.

Hansen, J. E., and M. Sato, 2001: Trends of measured climate forcing agents, Proc. Natl. Acad. Sci. U.S.A., 98, 14,778–14,783.Kiehl, J. T., 2007: Twentieth century climate model response and climate sensitivity, *Geophys. Res. Lett.*, 34, L22710, doi:10.1029/2007GL031383.

Lilly, D. K., 1968: Models of cloud-topped mixed layers under a strong inversion. *Quart. J. Roy. Meteor. Soc*., 94, 292-309.

Liu, H. L., W. Y. Lin, M. H. Zhang, 2010: Heat Budget of the Upper Ocean in the South-Central Equatorial Pacific. *J. Climate*, 23, 1779–1792. doi: 10.1175/2009JCLI3135.1

Meehl, G.A., et al., 2007: Global Climate Projections. In: Climate Change 2007: The Physical Science Basis. Contribution of Working Group I to the Fourth Assessment Report of the Intergovernmental Panel on Climate Change [Solomon, S., D. Qin, M. Manning, Z. Chen, M. Marquis, K.B. Averyt, M. Tignor and H.L. Miller (eds.)]. Cambridge University Press, Cambridge, United Kingdom and New York, NY, USA.

Ostrovskii, A. G. and L. I. Piterbarg, 2000: Inversion of Upper Ocean Temperature Time Series for Entrainment, Advection, and Diffusivity. *J. Phys. Oceanogr*., 30, 201–214.

Ramanathan, V., 1987: The role of earth radiation budget studies in climate and general circulation research, *J. Geophys. Res*., 92, 4075-4095.

Randall, D. A. et al., 2007: Climate models and their evaluation. In *Climate Change 2007*: The physical science basis. Contribution of working group I to the 4th assessment report of the IPCC. Cambridge University Press, Cambridge, United Kingdom and New York, NY, USA.

Raper, S. C. B., J. M. Gregory, and T. J. Osborn, 2001: Use of an upwelling-diffusion energy balance climate model to simulate and diagnose A/OGCM results, Clim. Dyn., 17, 601–613.

Schlesinger, M. E., 1988: Quantitative analysis of feedbacks in climate model simulations of CO2 induced warming, in *Physically-based Modeling and Simulation of Climate and Climate Change*, NATO ASI series, edited by Schlesinger, M. E., pp. 653-735, Kluwer Academic Press, 1988.

Senior, C. A., and J. F. B. Mitchell, 1993: Carbon dioxide and climate: the impact of cloud parameterization. *J. Climate*, 6, 5-21.

Soden, B. J., A. J. Broccoli, R. S. Hemler, 2004: On the Use of Cloud Forcing to Estimate Cloud Feedback. *J. Climate*, 17, 3661–3665.

Soden, B. J. and I. M. Held, 2006: An Assessment of Climate Feedbacks in Coupled Ocean–Atmosphere Models. *J. Climate*, 19, 3354–3360. doi: 10.1175/JCLI3799.1

Soden, B. J., I. M. Held, R. Colman, K. M. Shell, J. T. Kiehl, C. A. Shields, 2008: Quantifying Climate Feedbacks Using Radiative Kernels. *J. Climate*, 21, 3504–3520. doi: 10.1175/2007JCLI2110.1

Schwartz, S. E., 2007: Heat capacity, time constant, and sensitivity of Earth's climate system. JOURNAL OF GEOPHYSICAL RESEARCH, VOL. 112, D24S05, doi:10.1029/2007JD008746.

Wyant, M. C., C. S. Bretherton, J. T. Bacmeister, J. T. Kiehl, I. M. Held, M. Zhao, S. A. Klein, and B. A. Soden, 2006: A comparison of low-latitude cloud properties and their response to climate change in three AGCMs sorted into regimes using mid-tropospheric vertical velocity. *Climate Dyn.*, 27, 261-279.

Wetherald, R. T., and S. Manabe, 1988: Cloud feedback processes in general circulation models, *J. Atmos. Sci*., 45, 1397-1415.

Wigley, T. M. L., 2005: The climate change commitment, Science, 307, 1766– 1769.

Zhang, M. H., J. J. Hack, J. T. Kiehl and R. D. Cess, 1994: Diagnostic study of climate feedback processes in atmospheric general circulation models. *J. Geophys. Res.*, 99, 5525-5537.

Figure Captions

Figure 1. (a) 20th century simulation of globally averaged surface temperature anomalies from the NCAR CCSM3 and the GFDL CM2 and from observations. (b) Climate forcing of the 20th century from greenhouse gases (GHG), the sum of greenhouse gases and tropospheric aerosols (GHG+Aer), and total forcing from greenhouse gases, tropospheric aerosols, solar variability and volcanic forcing.

Figure 2. Change of cloud forcing in equilibrium climate change simulations normalized by a unit change of averaged surface temperature from 60^{o}S to 60^{o}N (unit in W/m^2/K). (a) NCAR CCSM3. (b) GFDL CM2.

Figure 3. Schematics of the three components of the model

Figure 4. (a) Projected climate forcing for the 21st century from the IPCC A1B and B1 scenarios. (b) Idealized forcing in this paper (solid blue).

Figure 5. Equilibrium (dashed) and transient (solid) response of surface temperature to external forcing without a deep ocean. Red and blue represent positive and negative cloud feedbacks of 0.75 W/m^2/K and -0.75W/m^2/K respectively; black represents zero cloud feedback. (a) The first 50 years. (b) The entire 150 years.

Figure 6. (a) Equilibrium (dashed) and transient (solid) response of surface temperature to external forcing with a deep ocean, color scheme is the same as in Figure 5. (b) Heat fluxes from the forcing (green), into the ocean (solid lines in red, black, and blue), loss through the atmosphere (dashed lines in red, black, and blue), and heat storage in the

mixed layer (dotted lines). Red and blue represent positive and negative cloud feedbacks of 0.75 W/m2/K and -0.75W/m2/K respectively; black represents zero cloud feedback.

Figure 7. Heat flux into the deep ocean as a function of heat storage in the mixed layer for two cloud feedbacks.

Figure 8. Vertical distribution of temperature in the deep ocean plotted for every 20 years. Numbers denote the time of year. (a) positive cloud feedback of 0.75 $W/m^2/K$; (b) no cloud feedback; (c) negative cloud feedback of -0.75$W/m^2/K$.

Figure 9. Sensitivity of transient surface temperature to model parameters. Solid lines are for parameters of the control case; dashed lines are for perturbed parameters. (a) Entrainment velocity is reduced from $w_e=10\times10^{-6}$ m/s to $w_e=5\times10^{-6}$ m/s. (b) Heat diffusivity is reduced from $k=1\times10^{-4}$ m/s to 0.5×10^{-4} m/s. (c) Upwelling velocity is increased from zero to 10 m/year. The color scheme is the same as in previous figures.

Figure 10. Solid lines are the same as in Figure 8a. Dashed lines are for reduced diffusivity in (a), and increased upwelling in (b).

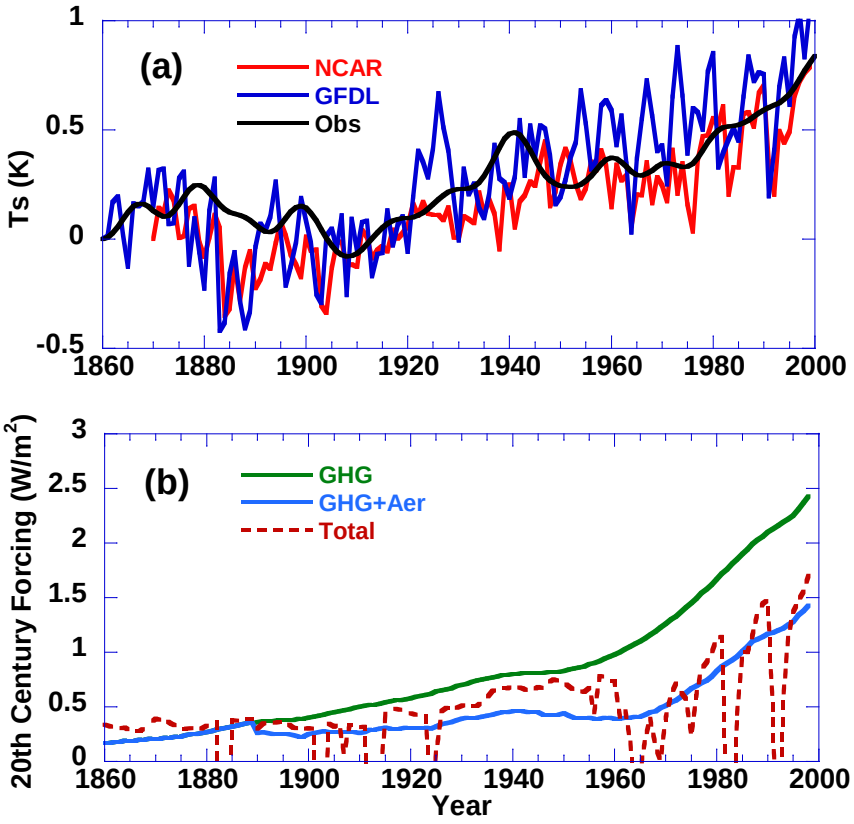

Figure 1. (a) 20th century simulation of globally averaged surface temperature anomalies from the NCAR CCSM3 and the GFDL CM2 and from observations. (b) Climate forcing of the 20th century from greenhouse gases (GHG), the sum of greenhouse gases and tropospheric aerosols (GHG+Aer), and total forcing from greenhouse gases, tropospheric aerosols, solar variability and volcanic forcing.

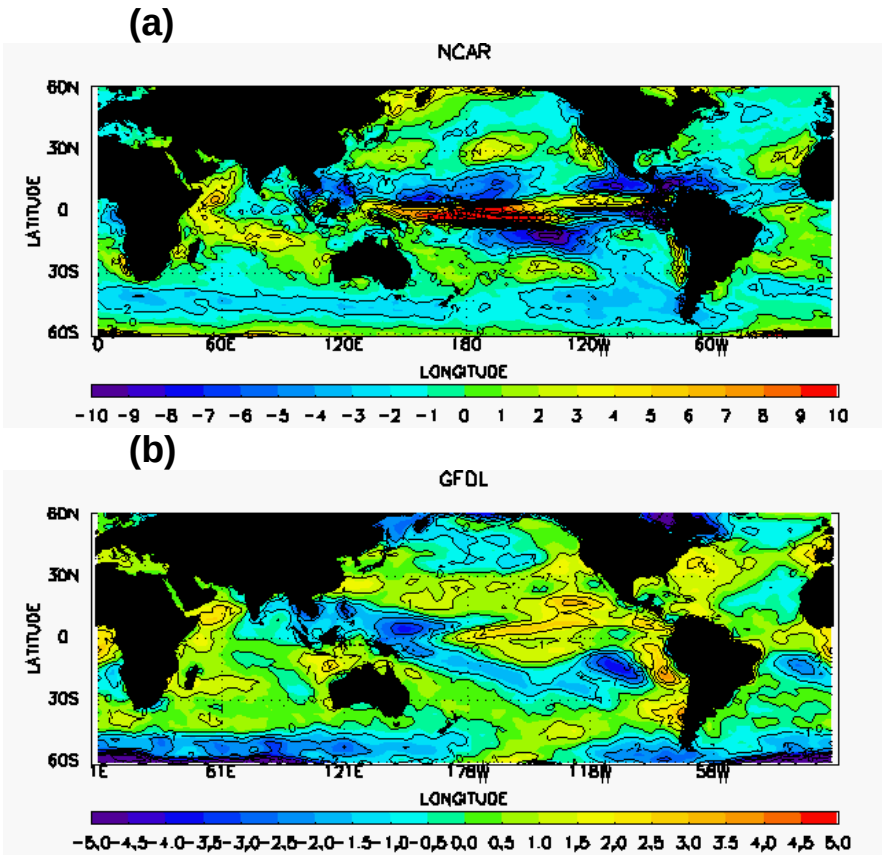

Figure 2. Change of cloud forcing in equilibrium climate change simulations normalized by a unit change of averaged surface temperature from 60^{o}S to 60^{o}N (unit in W/m^{2}/K). (a) from the NCAR CCSM3; (b) from the GFDL CM2.

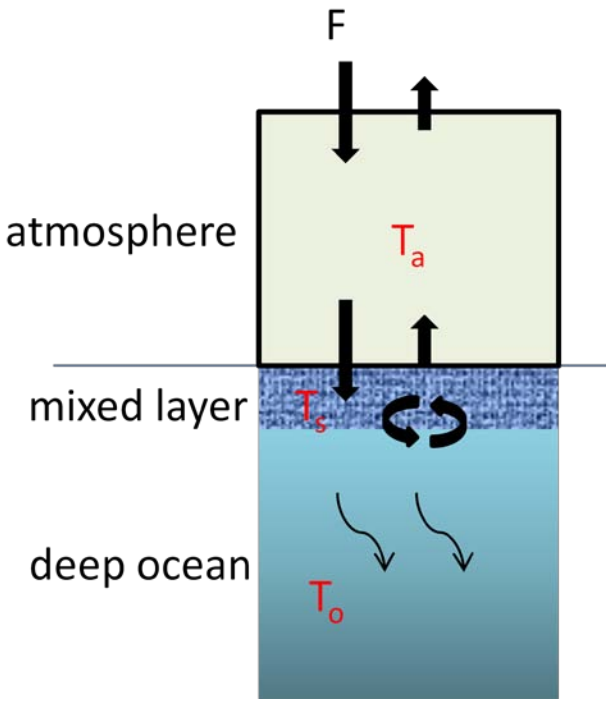

Figure 3. Schematics of the three components of the model

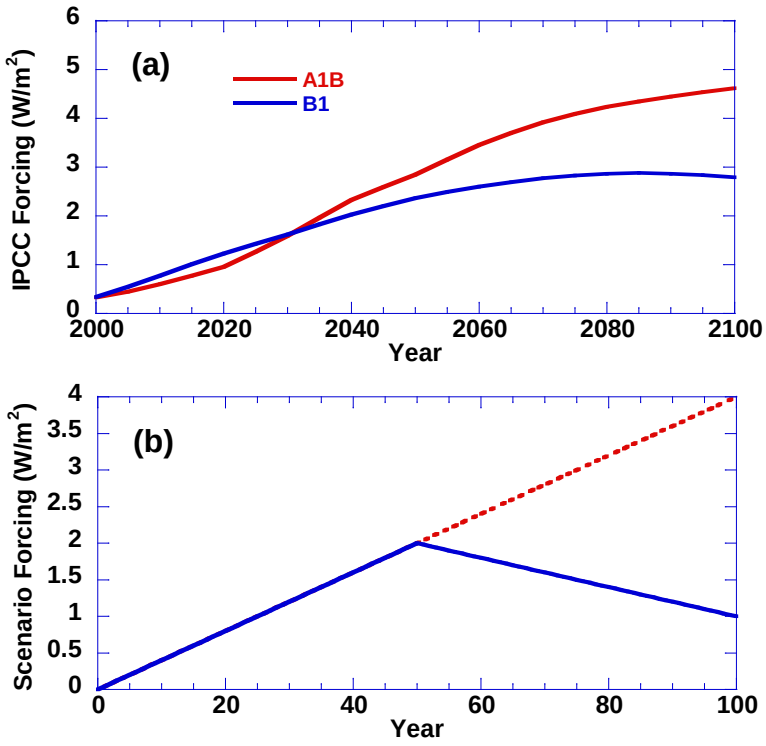

Figure 4. (a) Projected climate forcing for the 21st century from the IPCC A1B and B1 scenarios. (b) Idealized forcing used in this paper (solid blue).

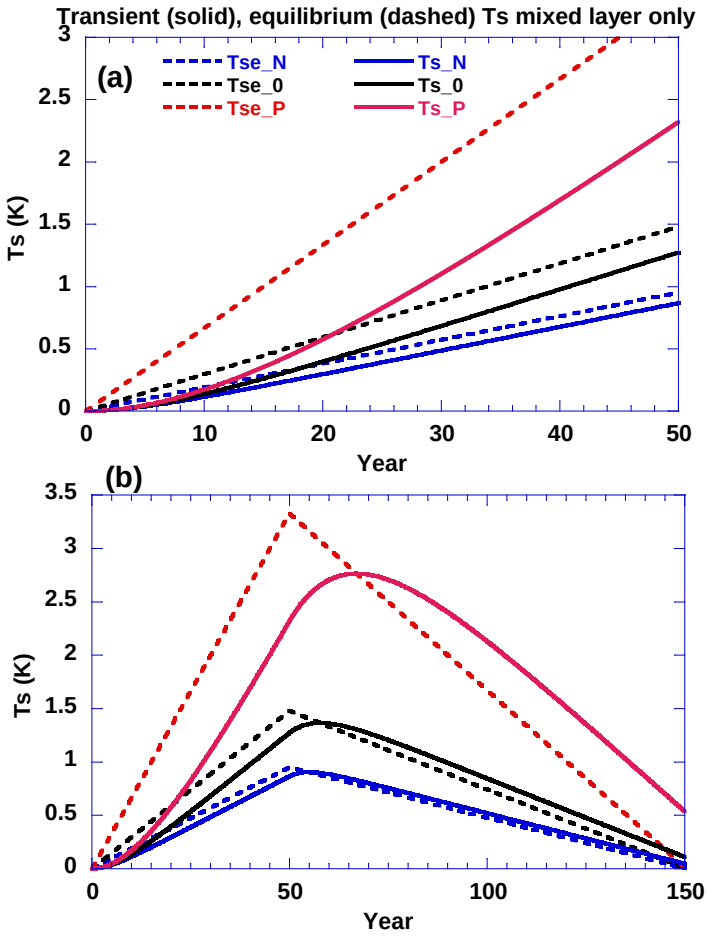

Figure 5. Equilibrium (dashed) and transient (solid) response of surface temperature to external forcing without a deep ocean. Red and blue represent positive and negative cloud feedbacks of 0.75 W/m^2/K and -0.75W/m^2/K respectively; black represents zero cloud feedback. (a) The first 50 years. (b) The entire 150 years.

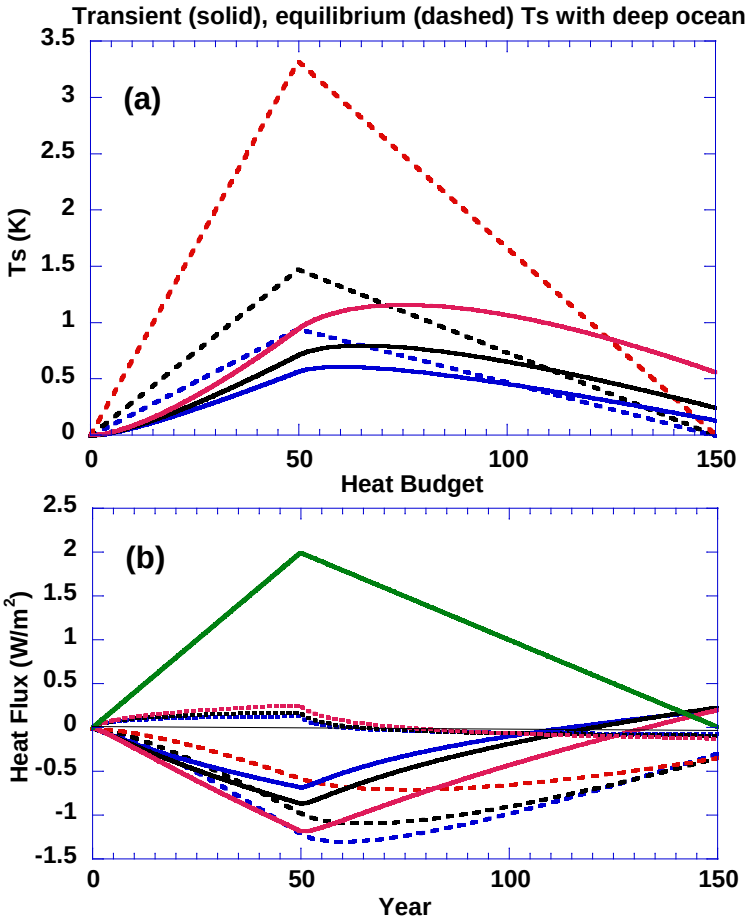

Figure 6. (a) Equilibrium (dashed) and transient (solid) response of surface temperature to external forcing with a deep ocean, color scheme is the same as in Figure 5. (b) Heat fluxes from the forcing (green), into the ocean (solid lines in red, black, and blue), loss through the atmosphere (dashed lines in red, black, and blue), and heat storage in the mixed layer (dotted lines). Red and blue represent positive and negative cloud feedbacks of 0.75 W/m2/K and -0.75W/m2/K respectively; black represents zero cloud feedback.

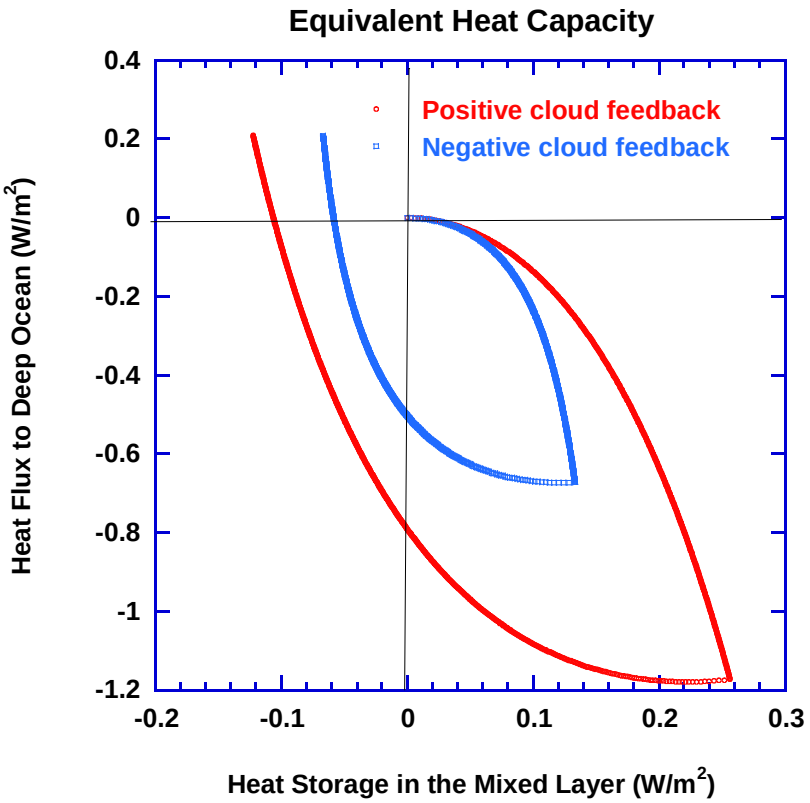

Figure 7. Heat flux into the deep ocean as a function of heat storage in the mixed layer for two cloud feedbacks.

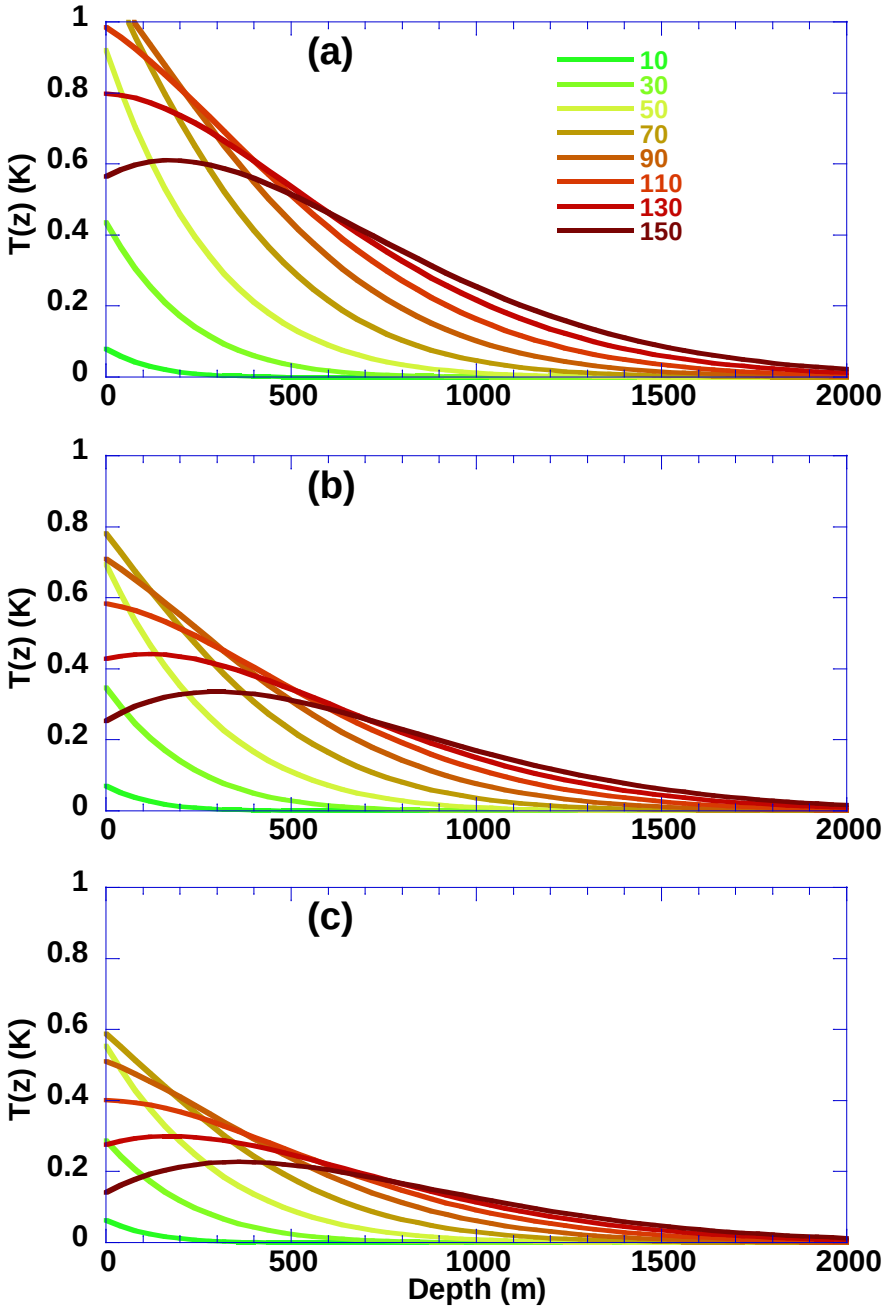

Figure 8. Vertical distribution of temperature in the deep ocean plotted for every 20 years. Numbers denote the time of year. (a) positive cloud feedback of 0.75 W/m^2/K ; (b) no cloud feedback; (c) negative cloud feedback of -0.75W/m^2/K.

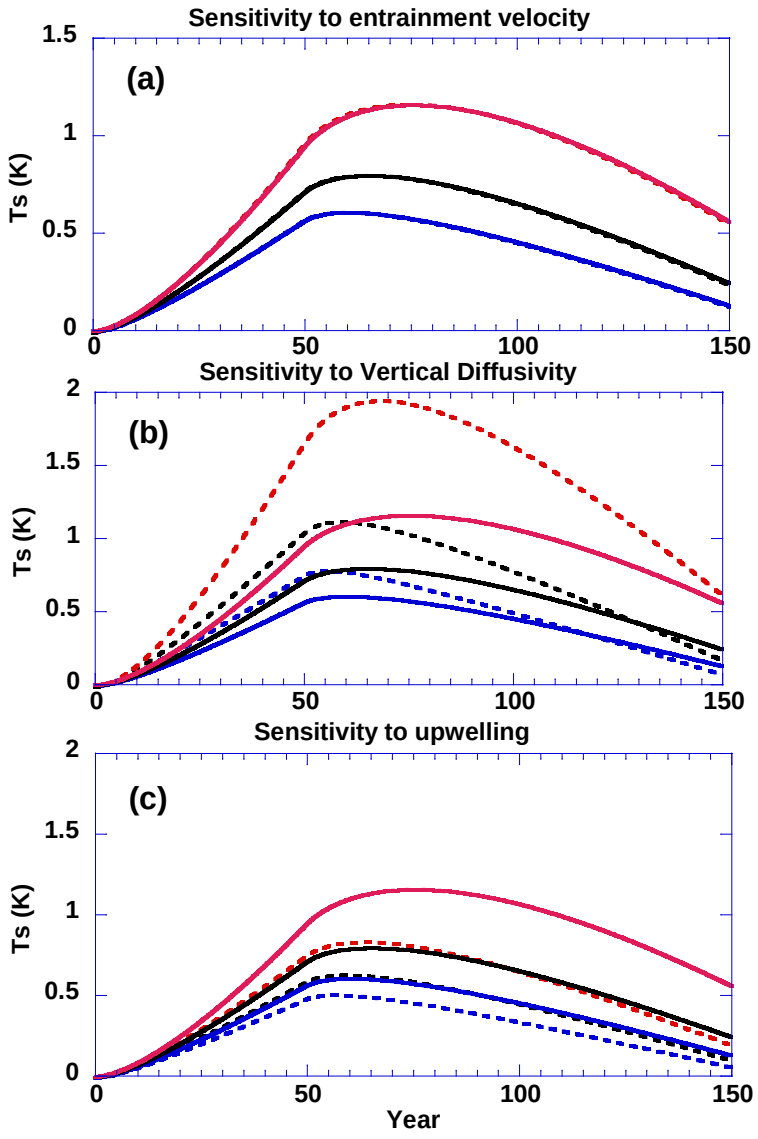

Figure 9. Sensitivity of transient surface temperature to model parameters. Solid lines are for parameters of the control case; dashed lines are for perturbed parameters. (a) Entrainment velocity is reduced from w_e=10×10^{-6} m/s to w_e=5×10^{-6} m/s. (b) Heat diffusivity is reduced from k=1×10^{-4} m/s to 0.5×10^{-4} m/s. (c) Upwelling velocity is increased from zero to 10 m/year. The color scheme is the same as in previous figures.

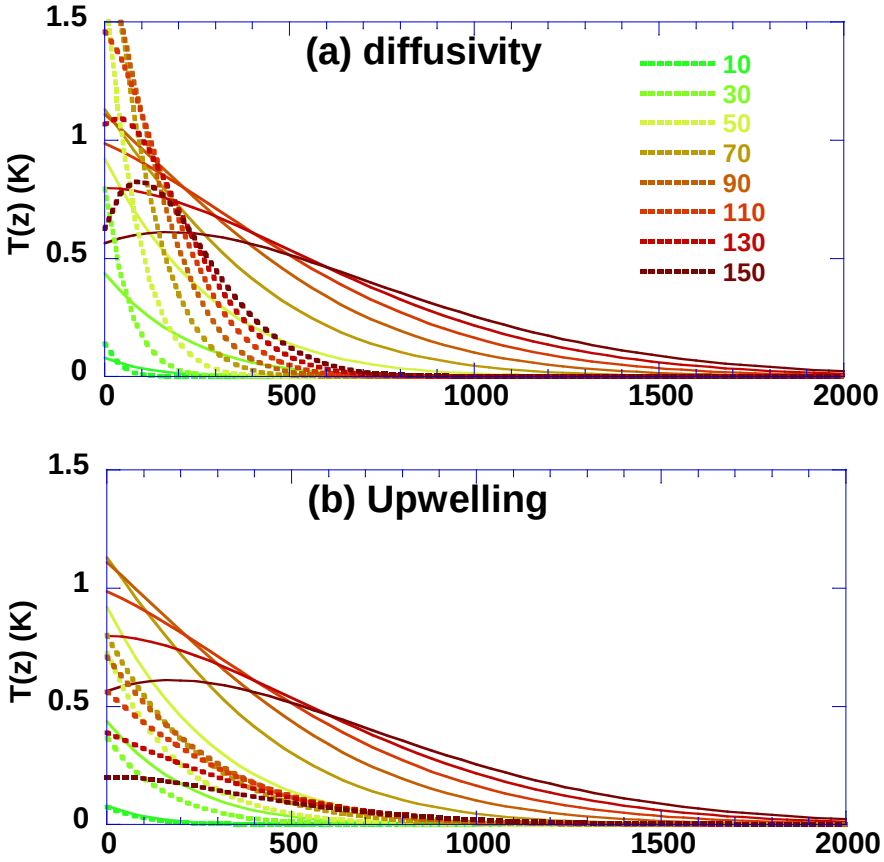

Figure 10. Solid lines are the same as in Figure 8a. Dashed lines are for reduced diffusivity in (a), and increased upwelling in (b).